

# OVATION-SM: A model of auroral precipitation based on SuperMAG generalized auroral electrojet and substorm onset times

E. J. Mitchell,<sup>1</sup> P. T. Newell,<sup>1</sup> J. W. Gjerloev,<sup>1,2</sup> and K. Liou<sup>1</sup>

Received 31 October 2012; revised 17 May 2013; accepted 17 May 2013; published 19 June 2013.

[1] OVATION-SM, an empirical model for different types of auroral energy flux, has been developed. OVATION-SM is a linear combination of the SME index (or square root of SME index for monoenergetic auroras), time since the last substorm onset, and time until the next substorm onset. Because OVATION-SM is based on ground magnetometer data and products of that data, it is possible to calculate continuous auroral power at a 1 min cadence for 30+ years. OVATION-SM captures the gross auroral morphology, including onsets and other brightening and dimming events. The detailed spatial auroral morphology is beyond the scope of the current version of OVATION-SM. OVATION-SM explains more than 70% of the variance in Polar UV Imager nightside auroral power, which makes it a better predictor of nightside auroral power than any other model currently available.

**Citation:** Mitchell, E. J., P. T. Newell, J. W. Gjerloev, and K. Liou (2013), OVATION-SM: A model of auroral precipitation based on SuperMAG generalized auroral electrojet and substorm onset times, *J. Geophys. Res. Space Physics*, 118, 3747–3759, doi:10.1002/jgra.50343.

## 1. Introduction

[2] Auroral precipitation is a direct effect of magnetosphere-ionosphere (M-I) coupling. Knowledge of auroral precipitation/power during substorms is a part of understanding M-I coupling. Auroral precipitation and its power can be measured by a number of methods, each with its advantages and disadvantages. In an ideal world, measurements of auroral precipitation would be the following: (1) global, covering at least one full hemisphere; (2) instantaneous; (3) continuous, with no gaps in time; and (4) detailed, giving auroral type and local distribution in high cadence.

[3] Currently, global imagers can collect an almost instantaneous measurement of auroral emissions, but cannot distinguish the type of auroral precipitation. They are also limited in spatial/temporal resolution and continuity of coverage. In situ particle measurements can distinguish the type of the auroral precipitation in an exact location on a high-temporal resolution, but are limited to the exact location of the satellite and cannot account for temporal changes between measurements. Ground-based imagers provide semi-continuous coverage in almost instantaneous measurements for a portion of the sky. Thus, they provide more detailed knowledge of temporal structures than in situ measurements as well as a

more continuous coverage than either type of satellite coverage, but they are not global and they are subject to many limitations, including cloud coverage and moonlight. Therefore, no single method of collecting auroral precipitation data gives all the information necessary to examine auroral power during a substorm.

[4] To resolve these measurement limitations, models of auroral precipitation are constructed from the available data. These models can be based on the following: the  $Kp$  index (a 3 h measure of magnetic activity) [Hardy *et al.*, 1985, 1991], the solar wind speed and interplanetary magnetic field [Brautigam *et al.*, 1991], a solar wind coupling function (Ovation Prime) [Newell *et al.*, 2009, 2010b], in situ measurements [Evans, 1987], and other input measurements. Newell *et al.* [2010a] showed that these four auroral precipitation models (Hardy  $Kp$  model, Brautigam IMF-based model, OVATION Prime, and Evans Nowcast model) cannot explain more than 58% of hourly variance and less of the minute-by-minute variance. The reason is that the models are based on inputs that do not capture the sudden substorm onset and the resulting changes in auroral power [Newell *et al.*, 2001, 2010a]. In their concluding remarks, Newell *et al.* [2010a] suggested that the only way to significantly improve the auroral precipitation models is with substorm onset timing and development criteria, which were not available at the time of publication.

[5] In July of 2011, SuperMAG (a global ground-based magnetometer database) released a generalized auroral electrojet index (SME index) [Gjerloev, 2012]. The original auroral electrojet (AE) index used 12 magnetometers spaced around the 40–80° magnetic latitude, and was the difference between the most positive (auroral electrojet upper envelope = AU) and most negative (auroral electrojet lower envelope = AL) local magnetic north perturbations of the 12

<sup>1</sup>The Johns Hopkins University Applied Physics Laboratory, Laurel, Maryland, USA.

<sup>2</sup>Department of Physics and Technology, University of Bergen, Bergen, Norway.

Corresponding author: E. J. Mitchell, The Johns Hopkins University Applied Physics Laboratory, 11100 Johns Hopkins Rd. 200-W254, Laurel, MD 20723, USA. (elizabeth.mitchell@jhuapl.edu)

stations for a given moment in time [Davis and Sugiura, 1966]. The SME index was generalized by increasing the number of contributing stations located between 40 and 80° magnetic latitude to 20–130 stations (depending on the year). Newell and Gjerloev [2011a] showed that the SME index explains  $\sim 3/4$  of the variance of nightside auroral power [Newell and Gjerloev, 2011a, Figure 7]. Newell and Gjerloev [2011a] also found that substorm onset can be identified by the SuperMAG generalized auroral electrojet lower envelope (SML) index. With the advent of both a high cadence (1 min) ground-based magnetic index and a continuous substorm onset list for 30+ years, the obstacles to a better auroral precipitation model were removed.

[6] Using the SME index and SuperMAG substorm onset list in conjunction with the DMSP (Defense Meteorological Satellite Program) particle data, a new auroral precipitation model (OVATION-SM) is constructed through multiple linear regression and stepwise regression. OVATION-SM finds the auroral power in 0.25 h by 0.5° bins above 50° magnetic latitude for four different types of auroras. Separation by auroral type allows the community to explore new questions specific to auroral type as well as substorm timing. This paper discusses both the construction of OVATION-SM and the existence of an increase in ion auroral precipitation prior to substorm onset. Section 2 explains the data used and the methodology employed in constructing OVATION-SM. Section 3 discusses OVATION-SM (the new auroral power model), measuring its ability to model auroral power. Section 4 discusses details captured by OVATION-SM, including ion auroras during the growth phase. Sections 5 and 6 provide a succinct statement of the conclusions and the future work to be done on OVATION-SM.

## 2. Data and Methodology

[7] Data from January 1984 to December 2005 are analyzed to construct OVATION-SM, including the SuperMAG generalized auroral electrojet index (SME) (section 2.1), the SuperMAG substorm onset list (section 2.2), and the auroral energy flux separated by auroral precipitation type based on the DMSP SSJ/4 detector data (section 2.3). Auroral energy flux is binned by magnetic local time, magnetic latitude, and the type of auroral precipitation that created it. The four types of auroral precipitation are as follows: discrete monoenergetic auroras (section 2.3.1), discrete broadband auroras (section 2.3.2), diffuse electron auroras (section 2.3.3), and ion auroras (section 2.3.4). Each bin of data is subjected to a stepwise regression through multiple linear regression analysis using the least squares method to fit the auroral energy flux. The resulting equations are functions of the SME index value, the time from previous substorm onset, and the time until next substorm onset.

### 2.1. The SME Index (A Generalized AE Index)

[8] SuperMAG is a global collaboration of ground-based magnetometer data, combining data from over 300 separate magnetometer stations [Newell and Gjerloev, 2011a, 2011b; Gjerloev, 2012]. The data are from 30+ years of collection by different organizations [Gjerloev, 2012; supermag.uib.no]. Not all 300 stations have data for all 30+ years. The early years have as few as 20 stations contributing to the SME index; this is still 66% more than the original

auroral electrojet (AE) index. The data handling is fully explained by Gjerloev [2012], including the automated processing of the ground magnetometer data with error correction, temporal resampling, rotation into local coordinates, and baseline removal.

[9] The SME index is a generalized form of the classical auroral electrojet index (AE(12)=AU – AL). AE is based on only 12 stations [Davis and Sugiura, 1966]. The SME index is based on 20 to 130 stations spread all over the northern polar region between 40 and 80° magnetic latitude. Like AE(12), the SME index is the difference between the most positive (auroral electrojet upper envelope, SMU) and most negative (auroral electrojet lower envelope, SML) magnetic perturbations in the local magnetic north component seen at the selected stations. The larger number of magnetometer stations in the SME index provides a higher probability of a station being nearer the location of onset at the time of onset, thus, capturing the time and magnitude of the substorm with higher accuracy.

[10] The correlation between Polar UV Imager (UVI) nightside auroral power and the SME index is strong, with  $\sim 3/4$  of the variance of Polar UVI nightside auroral power explained by a linear relationship between it and the SME index [Newell and Gjerloev, 2011a]. Thus, the SME index provides a continuous measurement by which nightside auroral energy flux can be modeled.

### 2.2. The SuperMAG Substorm Onset List

[11] Newell and Gjerloev [2011a] find that substorm onsets can be automatically identified using the SML index. Their SML-based substorm onset identification algorithm finds more than 53,000 substorm onsets between 1 January 1980 and 31 December 2009.

[12] Using the 1 min cadence SML index in a sliding 30 min buffer, Newell and Gjerloev [2011a] identify substorm onset as  $t_0$  when the following conditions are met:

$$\text{SML}(t_0 + 1) - \text{SML}(t_0) < -15 \text{ nT} \quad (1)$$

$$\text{SML}(t_0 + 2) - \text{SML}(t_0) < -30 \text{ nT} \quad (2)$$

$$\text{SML}(t_0 + 3) - \text{SML}(t_0) < -45 \text{ nT} \quad (3)$$

$$\sum_{i=4}^{30} \frac{\text{SML}(t_0 + i)}{26} - \text{SML}(t_0) < -100 \text{ nT} \quad (4)$$

[13] These conditions force the drop in the SML index to be sharp and sustained for a minimum of 30 min. Typically, these substorm onsets lag no more than 4 min behind the corresponding onset identified by Polar UVI data [Newell and Gjerloev, 2011a].

[14] Substorm onset identification provides two important capabilities in modeling auroral power:

[15] 1. continuous identification of substorm onsets, and

[16] 2. precise identification of when an event occurs.

[17] Continuous identification of substorm onsets allows substorms to be classified as recurrent or isolated. Newell and Gjerloev [2011b] find that there are two distinct populations of substorm time intervals, the group with less than 82 min between onsets (recurrent) and the group with greater than 3 h between onsets (isolated). Only the isolated

substorms are used to construct OVATION-SM. This removes the possibility of overlapping between recovery and growth phases, which could hide or blur growth phase events. Under these conditions, 14,434 substorm onsets are identified using the SuperMAG database.

[18] Precise identification of when an event occurs allows growth phase events to be identified, such as pre-onset particle precipitation. By fitting the data with time since last onset and time until next onset, the model is able to evaluate previously hidden growth phase events. Thus, along with the SME index, times to and from substorm onsets are used.

### 2.3. DMSP Particle Data

[19] To model location- and type-dependent auroral energy flux, particle precipitation data need to be separated into types: ion or electron, diffuse or discrete, and monoenergetic or broadband (types of discrete aurora). Particle precipitation data come from the SSJ/4 electrostatic analyzers on the DMSP F06 through F15 satellites and the SSJ/5 detector on the F16 satellite. The data are from 1 January 1984 to 31 December 2005, a period of 22 years covering two solar cycles.

[20] The DMSP flies a series of low-altitude satellites in Sun-synchronous, circular polar orbits at ~845 km altitude, with orbital inclinations of 98.7°. The DMSP orbits loosely align along the 0600–1800 and 0900–2100 local time lines, which cause the coverage to be denser in the prenoon and premidnight sectors and sparser in the postnoon and postmidnight sectors except at high latitudes. The SSJ/4 and SSJ/5 detectors are curved plate electrostatic analyzers, which measure electrons and ions of energies between 30 eV and 30 keV. The instrumentation gathers a complete spectrum every second. At high latitudes used in this study, the three-axis stabilized design of the satellites allows the detectors to gather a majority of the data from the loss cone. Each spectrum is assigned an auroral type using the algorithms set out by *Newell et al.* [2009].

#### 2.3.1. Monoenergetic Aurora Identification

[21] Monoenergetic auroras are discrete electron auroras formed by electron acceleration from quasi-static field-aligned electric fields [*Frank and Ackerson, 1971*]. A DMSP particle spectrum is classified as monoenergetic when (1) the differential energy flux is greater than  $10^8$  eV/(cm<sup>2</sup> s sr eV) at the peak channel, (2) the differential energy flux drops 60% or more within two energy channels of the peak differential energy flux channel on both sides, and (3) the average energy is greater than 80 eV while the differential energy flux peak is greater than 100 eV. For an in-depth review of the algorithm, see *Newell et al.* [2009].

#### 2.3.2. Broadband (Wave) Aurora Identification

[22] Broadband (wave) auroras are discrete auroras formed by electron acceleration from dispersive Alfvén waves [*Chaston et al., 2003, 2004, 2007*]. A DMSP particle spectrum is classified as broadband when (1) three or more channels have a differential energy flux of greater than  $2.0 \times 10^8$  eV/(cm<sup>2</sup> s sr eV), (2) one or more of the greater than  $2.0 \times 10^8$  eV/(cm<sup>2</sup> s sr eV) differential energy flux channels are equal to 140 eV or higher (300 eV or higher for  $9.5 <$  magnetic local time (MLT)  $< 14.5$ ), (3) the average energy is greater than 80 eV, and (4) the spectrum does not satisfy the monoenergetic criteria. For an in-depth review of the algorithm, see *Newell et al.* [2009].

#### 2.3.3. Diffuse Electron Aurora Identification

[23] Diffuse electron auroras are all electron auroras that have not been accelerated. A DMSP particle spectrum is classified as diffuse when it is not classified as either monoenergetic or broadband. This classification ensures all DMSP electron spectra are used in this study.

#### 2.3.4. Ion Aurora Identification

[24] There is no similar classification scheme for ions. All ion DMSP particle spectra are classified as ion auroras regardless of how the electron auroras are classified.

[25] The measured DMSP ion and diffuse electron auroras spectra are known not to cover the entire energy range, having significant fractions of their energy fluxes above 30 keV [*Newell et al., 2009*]. Both ion and electron populations have been shown to have kappa distributions in the magnetotail [*Christon et al., 1991; Wing and Newell, 1998; Kletzing et al., 2003*] and in diffuse precipitation. Kappa distributions are Maxwellian distributions with high-energy tails. Because a significant fraction of their energy fluxes are above 30 keV, both the ion and diffuse electron spectra may be extrapolated to 50 keV using a simple Maxwellian fit. This extrapolation is used here. For more on the reasoning behind the extrapolation and methodology, refer to the discussion by *Newell et al.* [2009].

### 2.4. Polar UV Imager Nightside Auroral Power

[26] The Polar UVI is a large aperture ( $f/2.9$ ), narrow-angle (8° circular field of view) imager with a spatial resolution of 0.04° per pixel. In 1996 and 1997, Polar UVI monitored the Northern Hemisphere for ~9 h out of its 18 h orbital period. A detailed description of the spacecraft and instrument is provided by *Torr et al.* [1995].

[27] The Lyman-Birge-Hopfield long filter (LBHL) on Polar UVI is centered on the 170 nm line, measuring the molecular nitrogen bands. The response of the molecular nitrogen bands is proportional to the total electron energy flux of particles above a few hundred eV [*Strickland et al., 1983*]. LBHL intensity can be used to infer electron energy flux because electron impact is the only process that produces molecular nitrogen LBHL bands [*Holland, 1969*]. Thus, the auroral luminosity measured by the Polar UVI LBHL can be transformed into a measure of auroral energy flux. *Newell et al.* [2001, and references therein] provide a concise explanation on computing auroral energy flux associated with auroral luminosity.

[28] The Polar UVI auroral power (energy flux integrated over section of ionosphere) database used in this work was compiled by Kan Liou and has been discussed in several other places [e.g., *Liou et al., 1997, 1998; Newell et al., 2001, 2010a; Newell and Gjerloev, 2011a*]. *Liou et al.* [1997] discussed the creation of this database, including dayglow removal. Each Polar UVI nightside auroral power value is an integration of the energy flux over the entire nightside (1800 MLT to 0600 MLT) from 60° magnetic latitude to the magnetic pole. Only cases where the entire nightside oval is within the field of view were used in calculating Polar UVI nightside auroral power. Each Polar UVI dayside auroral power value is an integration of the energy flux over the entire dayside (0600 MLT to 1800 MLT) from 60° magnetic latitude to the magnetic pole. Only cases where the entire dayside oval is within the field of view were used in calculating Polar UVI dayside auroral power.

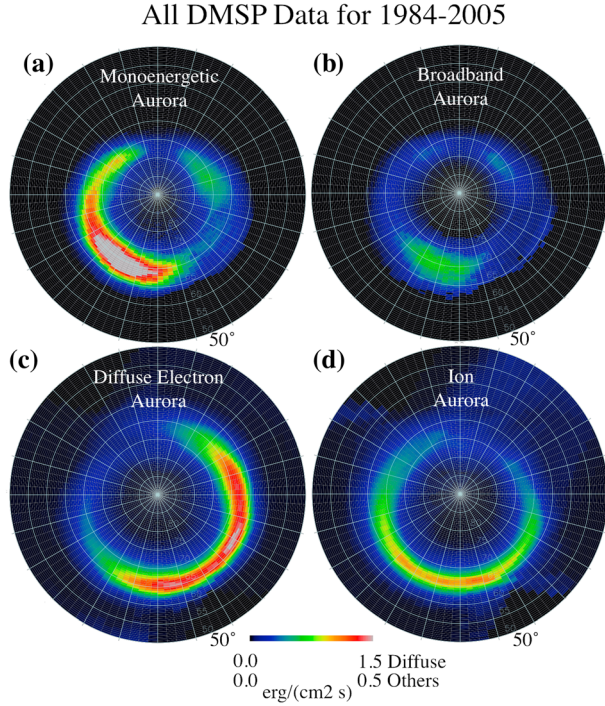


**Figure 1.** (a–d) Average DMSP energy fluxes in OVATION-SM for each auroral type.

## 2.5. Construction of OVATION-SM

[29] OVATION-SM is constructed from the DMSP spectra described above. Each DMSP spectrum is associated with an auroral type (AT), a magnetic local time (MLT), a magnetic latitude (MLAT), an SME index value (SME), a time since the last substorm onset ( $T1$ ), and a time until the next substorm onset ( $T2$ ). For monoenergetic auroras, the square root of the SME index ( $\sqrt{\text{SME}}$ ) is used [Newell and Gjerloev, 2011a]. Spectra from recurrent substorms ( $T1 - T2 < 3$  h) are removed from the populations.

[30] Although DMSP takes measurements from both hemispheres, OVATION-SM is constructed by combining both hemispheric data. As a result, it is hemispheric averaged. The method assumes that the aurora is hemispherically symmetric. This is not always true. Hemispheric asymmetry occurs in the afternoon auroras [Fillingim *et al.*, 2005] and during auroral breakups [Liou and Newell, 2010].

[31] There are four auroral types. MLT is split into 96 (0.25 h) bins. Magnetic latitude is split into 80 ( $0.5^\circ$ ) bins, spanning  $50^\circ$  to  $90^\circ$ . The hemispheres are combined by MLT and absolute value of MLAT. This gives a spatial grid resolution of 0.25 h by  $0.5^\circ$  with 7680 bins. Each spatial bin has four auroral types (4 AT).

[32] Each AT in each bin is fitted using stepwise regression and multiple linear regression with the least squares method of minimization ( $\sim 30,000$  equations). Stepwise regression is a method of determining which variables are significant alone and in combination. The possible energy flux ( $J_{Eik}$ ) is fit to SME,  $T1$ , and  $T2$ . The form of the fit is

$$J_{Eik}(\text{SME}, T1, T2) = \beta_{0,i,k} + \beta_{sme,i,k} * \text{SME} + \beta_{T1,i,k} * T1 + \beta_{T2,i,k} * T2 \quad (5)$$

where  $J_{E,i,k}$  is the possible energy flux ( $\text{erg cm}^{-2} \text{s}^{-1}$ ),  $i$  indexes the auroral type (AT),  $k$  indexes the geomagnetic bin (MLT, MLAT), SME is the SME index (nT),  $T1$  is the time since last substorm onset (seconds),  $T2$  is the time until the next substorm onset (seconds), and  $\beta_{0,i,k}$ ,  $\beta_{sme,i,k}$ ,  $\beta_{T1,i,k}$ , and  $\beta_{T2,i,k}$  are the coefficients calculated by the multiple linear regression analysis.

[33] Each multiple linear regression is weighted by the occurrence frequency of the auroral type in each geomagnetic bin. The occurrence frequency is the ratio of the number of times the auroral type occurred in that geomagnetic bin to the total number of auroral measurements made in that geomagnetic bin. The final auroral energy flux is the product of the multiple linear regression fit and the occurrence frequency in the form

$$J_{E,i,k}(\text{SME}, T1, T2) = j_{E,i,k}(\text{SME}, T1, T2) * f_{i,k} \quad (6)$$

where  $J_{E,i,k}$  is the auroral energy flux ( $\text{ergs cm}^{-2} \text{s}^{-1}$ ),  $j_{E,i,k}$  is the possible energy flux,  $i$  indexes the auroral type,  $k$  indexes the geomagnetic bin (MLT and MLAT), SME is the SME index,  $T1$  is the time since last substorm onset,  $T2$  is the time until the next substorm onset, and  $f_{i,k}$  is the occurrence frequency. Auroral power for a given bin is the surface area of the bin at 120 km altitude times  $J_{E,i,k}$ . Hemispheric auroral power is the summation of auroral power from the contributing bins.

## 3. OVATION-SM, an Empirical Model

[34] OVATION-SM is an empirical model, which uses the SME index and SML-derived substorm onset times to calculate the auroral energy flux. Before discussing any science questions addressed with model results, a review and validation of the model must be presented. Section 3.1 presents the data, correlation coefficients, and statistical significances for each bin. Section 3.2 discusses the morphology of OVATION-SM results, comparing them to Polar UVI images for the same substorm. Section 3.3 discusses the comparison of Polar UVI auroral power with OVATION-SM auroral power.

### 3.1. Data, Correlation, and Statistical Significance

[35] The average auroral energy fluxes for each type of aurora used in constructing OVATION-SM are plotted in Figure 1. Most of the energy flux for monoenergetic aurora is concentrated between 1900–2400 MLT and  $65^\circ$ – $75^\circ$  MLAT with a tail wrapping past dusk into the postnoon sector (Figure 1a). Most of the energy flux for broadband aurora is concentrated between 2030–0100 MLT and  $65^\circ$ – $75^\circ$  MLAT with two isolated spots on the dayside (Figure 1b). Most of the energy flux for diffuse electron aurora is concentrated between 2100–1000 MLT and  $60^\circ$ – $75^\circ$  MLAT (Figure 1c). Most of the energy flux for ion aurora is concentrated between 1900–0300 MLT and  $60^\circ$ – $70^\circ$  MLAT with both ends extending into the dayside (Figure 1d). These results agree well with Newell *et al.* [2009].

[36] When examining these plots, remember that they are the average of all the data used here, both during highly active times and quiet times. Thus, the average energy flux for broadband aurora suggests that broadband aurora contribute almost nothing. This is incorrect. Newell *et al.*

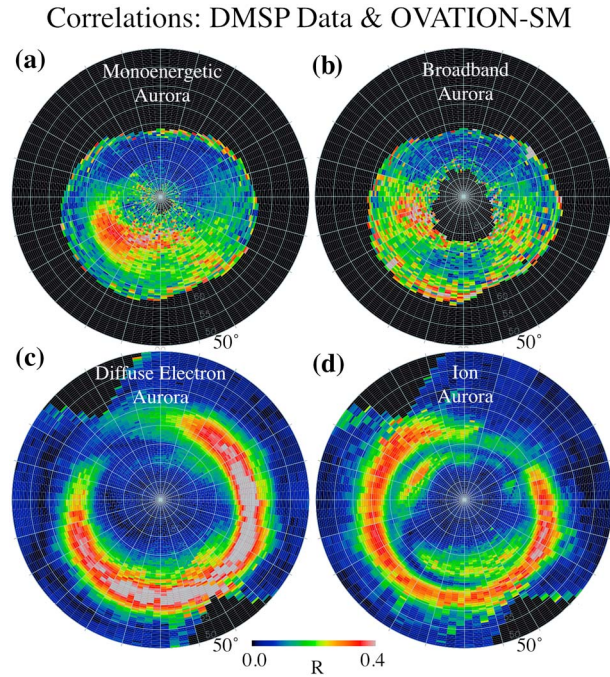


**Figure 2.** (a–d) Correlations between DSMP data and OVATION-SM for each auroral type.

[2010c] have shown that broadband aurora is extremely active in the first 30 min of a substorm. Yet when averaged over active and quiet times, the energy flux is blurred. Such averaging can also explain the tail into the dayside for monoenergetic aurora. *Newell et al.* [2009] showed monoenergetic energy flux increases in strength and spreads from 2100 MLT to 1500 MLT when the solar wind driving is increased. Thus, the data plots confirm that the energy flux used is reasonable, but does not explain the trends in auroras at different phases of a substorm.

[37] Stepwise regression and multiple linear regression analysis compute more than just the regression coefficients ( $\beta_0, \beta_{sme}, \beta_{T1},$  and  $\beta_{T2}$ ). They compute the correlations between the data and model as well as the statistical significances for each of the variables alone and in combination. Stepwise regression uses the statistical significance and the amount of explained variability by each variable alone or in combination to determine which variables are necessary for the model. Figure 2 shows the correlations for each bin with black representing no correlation or no data available and gray representing a correlation of better than 0.4.

[38] The higher correlation region for monoenergetic aurora is slightly poleward of the bulk of the energy flux (Figure 2a). There is not a strong correlation between monoenergetic energy flux and the square root of SME or substorm phase (as represented by time since/until substorm onset).

[39] There are no clear higher correlation regions for minute-by-minute DMSP broadband aurora (Figure 2b). If examined closely, the area of strong energy flux corresponds to an area of low correlation. This suggests that broadband auroras are only predictable at specific times.

[40] The higher correlation region for diffuse electron aurora completely encompasses the region of strong energy flux, expanding in both MLT and MLAT (Figure 2c). The strength of the correlations and the extent of the correlations

suggest that the diffuse electron auroral energy flux is well modeled by SME and the substorm phases as represented by time since/until substorm onset. This suggestion will be explored further throughout this work.

[41] The higher correlation region for ion aurora covers most of the region of strong energy flux (Figure 2d). On the duskside, the poleward edge of the strong energy flux is outside the region of high correlation. This area of low correlation on the poleward edge of the energy flux region is fairly well defined, suggesting that it is due to a nonlinear response rather than a lack of data or a lack of organization by SME and substorm phase. One possible explanation is the movement of the ion auroral boundaries around onset. *Mende et al.* [2003] showed that the ion auroral boundary moves equatorward prior to onset and then the area spatially near onset jumps poleward just after onset. This boundary movement would produce a nonlinear relationship between the timing and auroral energy flux, which in turn would decrease the correlation as seen in the premidnight sector between  $66.5^\circ$  and  $68.5^\circ$  MLAT.

[42] Figure 3 shows the number of statistically significant variables in the multiple linear regression analysis as determined by stepwise regression. When the fit is calculated, the statistical significance of each variable alone and in the presence of the others is calculated using the  $F$  test. The variables must remain significant in the presence of the others to be counted as significant. Thus, Figure 3 depicts how many variables are significant for each auroral type in the model. Blue indicates one variable is statistically significant, orange indicates two variables are statistically significant, and gray indicates three variables are statistically significant. If only one variable is statistically significant, then it is almost always

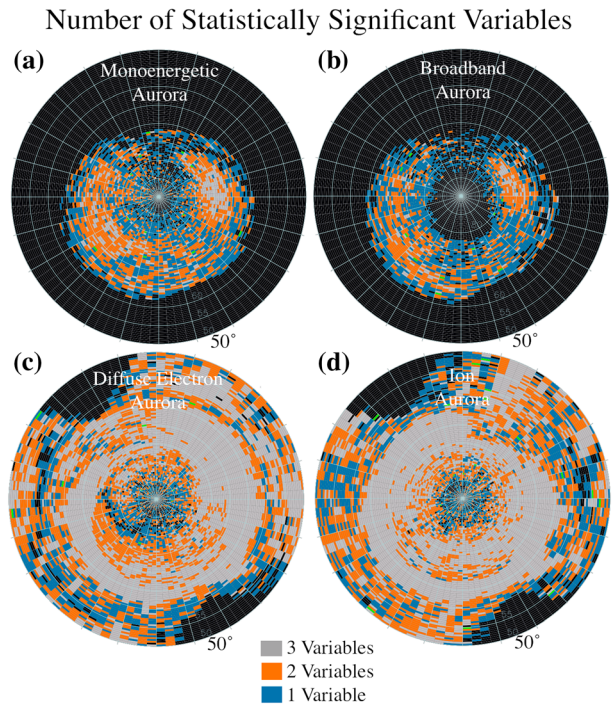


**Figure 3.** (a–d) Number of statistically significant variables in the multiple linear regression analysis used to make OVATION-SM for each auroral type.

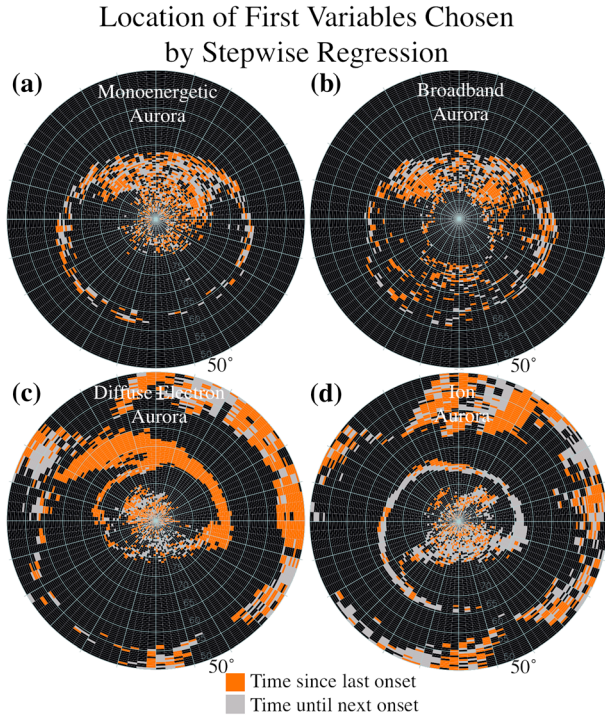


**Figure 4.** (a–d) First variables chosen by stepwise regression when constructing OVATION-SM for each auroral type. Black represents SME or no data, orange represents time since last substorm onset, and gray represents the time until the next substorm onset.

SME (or the square root of SME for monoenergetic aurora) on the nightside. If two variables are statistically significant, they are SME and one of the time variables on the nightside. On the dayside, stepwise regression often chooses one of the time variables first, meaning the simple linear regression between DMSP auroral energy flux and time explains more of the variability than the SME index does. Figure 4 shows the first variable chosen by stepwise regression in each bin. The SME index is black, the time since the last substorm onset is orange, and the time until the next substorm onset is gray.

[43] For monoenergetic auroral energy flux, the relationship with the square root of SME is statistically significant, especially on the nightside (Figures 3 and 4a). The second statistically significant variable chosen on the nightside varies, with time since last substorm onset being important on the duskside and time until next substorm onset being important on the dawnside. There is an isolated patch of all three variables being statistically significant in the prenoon sector. On the dayside, time becomes the first variable chosen with a mix of time since last onset and time until next onset (Figure 4a).

[44] For broadband auroral energy flux, the relationship with the SME index is statistically significant, especially on the nightside (Figures 3 and 4b). The few locations where two variables are statistically significant, the second variable is usually the time since last substorm onset. The time since last onset is often the first chosen variable on the dayside, frequently being the only statistically significant variable (Figures 3 and 4b). In the cusp region, where the definition of broadband aurora has been modified to remove false wave

aurora signatures (the 9.5 to 14.5 MLT criteria), the time until next onset becomes the first chosen variable (Figure 4b).

[45] Overall, the three variable models are unnecessary for discrete auroras. The discrete auroral models only need one or two of these variables to estimate the auroral energy flux. The three variable models are used to maintain uniformity for all the models.

[46] For diffuse electron auroral energy flux, all three variables are statistically significant for a majority of the auroral oval (Figure 3c). On the nightside and a majority of the dayside, SME is the first chosen variable (Figure 4c). On the dayside, there is a band where time since last onset becomes the first chosen variable. The band is high latitude and correlates to the eastward drift of electrons. The formation of such a band is unsurprising. As electrons drift eastward to the dayside, the magnetic field compression changes the loss cone pitch angle, allowing scattering into the ionosphere. It is expected that the auroral power will decrease with increasing time since last onset ( $T1$ ). Overall, the multiple linear regression analysis fit is well correlated as well as statistically significant for all three variables (Figures 2, 3, and 4c). This gives a high degree of confidence to analysis done with OVATION-SM for diffuse electron auroras.

[47] Likewise for ion auroral energy flux, all three variables are statistically significant over a majority of the auroral oval (Figure 3d). The time until next onset ( $T2$ ) variable is chosen first by the stepwise regression for a narrow band curving from 0500 MLT to 2300 MLT (Figure 4d). All three variables are statistically significant in this band (Figure 3d). The band of  $T2$  also corresponds to the well-defined edge between high and low correlation discussed above (Figure 2d). Further discussion of the role of this band appears later in the paper. Again, overall, the multiple linear regression analysis fit is well correlated as well as statistically significant for all three variables. This gives a high degree of confidence to analysis done with OVATION-SM for ion auroras.

### 3.2. Morphology

[48] There are two aspects of auroral models that need validation. One is the accurate portrayal of auroral morphology (gross and detailed). The other is an accurate prediction of magnitude/intensity of the auroral power. Auroral power gives the strength of auroral brightening but not specific location. Even when the detailed morphology cannot be established, accurate auroral power can provide useful information. This section discusses the morphology of OVATION-SM as compared with Polar UVI images. The following section discusses the auroral power of OVATION-SM as compared with that of Polar UVI.

[49] To examine the morphology of OVATION-SM as compared with Polar UVI images, all of the auroral types in OVATION-SM are combined into a single image, which is done by summing each bin over the auroral types. The weighted summation of auroral types is used because a given geomagnetic bin can contain several auroral types during a single satellite pass. The left-hand column of Figures 5a–5e contain five auroral energy flux maps ( $\text{ergs cm}^{-2} \text{s}^{-1}$ ) from the OVATION-SM modeling of the 18 December 1996 substorm with onset at 0534 UT. The right-hand column of Figures 5f–5j contain five auroral brightness images ( $\text{photons cm}^{-2} \text{s}^{-1}$ ) from Polar UVI. While the conversion from auroral luminosity to auroral energy flux is time-consuming, the major

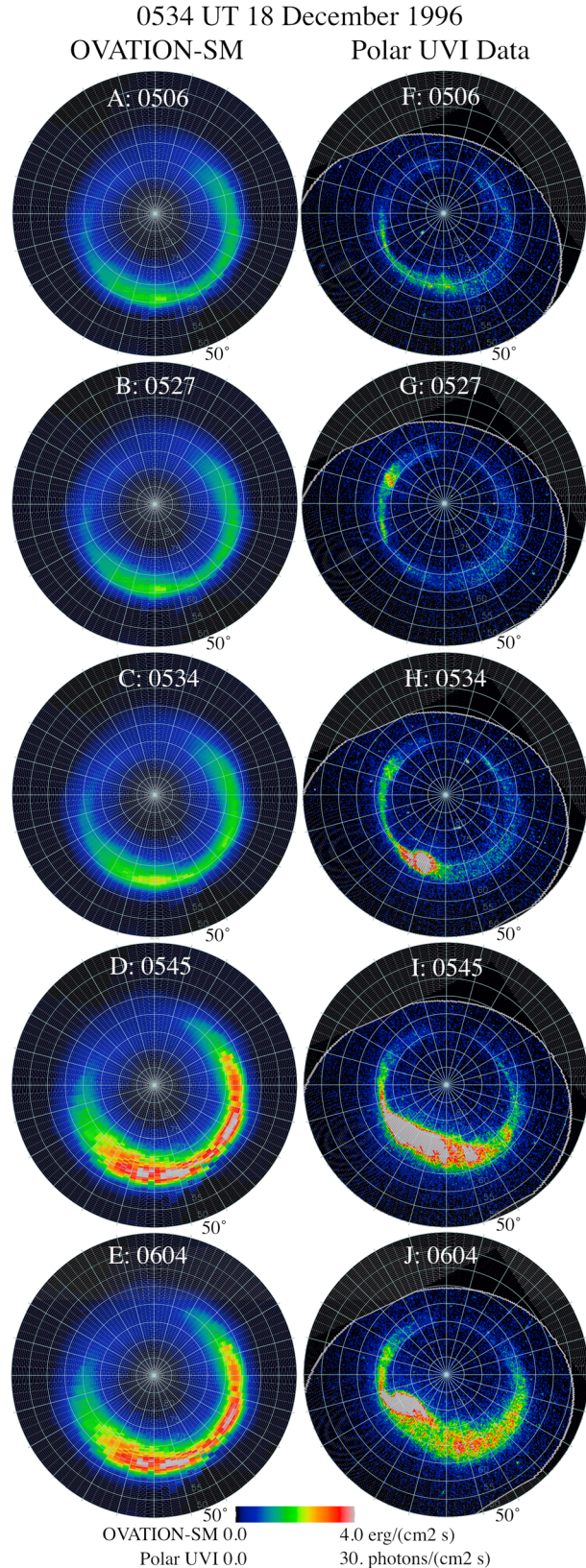


**Figure 5.** (a–j) OVATION-SM and Polar UVI data for the substorm with onset at 0534 UT on 18 December 1996.

morphological features should not change drastically between the Polar UVI images and the resulting map of the auroral energy flux. Thus, a comparison of the qualitative morphological features is possible without transforming the Polar UVI data into energy flux.

[50] OVATION-SM clearly captures gross morphology of the aurora. Both OVATION-SM and Polar UVI locate auroral activity above 60° MLAT with nightside aurora reaching lower MLAT than dayside. Both observations and model see decreased aurora around the magnetic pole (above 85° MLAT). Both OVATION-SM and Polar UVI see more night-side activity. It is the detailed morphology of the aurora that is not as well captured by OVATION-SM. This is expected, because OVATION-SM is based on three location-independent parameters (SME,  $T_1$ , and  $T_2$ ) to calculate a local energy flux (DMSP data). The next version of OVATION-SM will add MLT-dependent variables, allowing DMSP data to be linked to a more realistic magnetic field variation. This should capture more of the detailed morphology.

[51] The ionospheric maps in the first row of Figures 5a and 5f occur 28 min prior to substorm onset. Both images have minimal brightening near midnight. The ionospheric maps in the second row of Figures 5b and 5g occur 7 min prior to substorm onset. OVATION-SM shows an increase in auroral energy in the postmidnight sector while Polar UVI has auroral brightening in the premidnight and postnoon sectors. The ionospheric maps in the third row of Figures 5c and 5h occur at onset. OVATION-SM observes onset at midnight, expanding poleward between 2100 and 2300 MLT. Polar UVI observes onset at 2200–2300 MLT. Both OVATION-SM and Polar UVI see increase in auroral activity after substorm onset. Eleven minutes after onset, OVATION-SM has poleward expansion and auroral brightening throughout the nightside and into the prenoon sector, while Polar UVI sees poleward expansion and auroral brightening between 1800 and 0400 MLT (Figures 5d and 5i). By 30 min into the substorm, the gross morphology of OVATION-SM is not changing, just decreasing in intensity (Figure 5e). Polar UVI also sees the auroral brightness decreasing (Figure 5j).

[52] OVATION-SM captures the gross morphological changes, brightening, and dimming as the Polar UVI observations do. The detailed morphology (i.e., arcs and streamers) is beyond the scope of OVATION-SM at the present time. This is not an unexpected result. OVATION-SM is an empirical model based on three location-independent variables (the SME index, time since the last substorm onset, and time until the next substorm onset). Auroral morphology is a localized phenomenon, dependent on local currents, conductance, neutral densities, magnetic field structures, etc. It would be remarkable if a location-independent number could capture all of these details for all of the MLT sectors. High-cadence, MLT-dependent variables are expected to be able to capture the detailed morphology better. The addition of the high-cadence, MLT-dependent variables is future work, not explored here.

### 3.3. Auroral Power

[53] Auroral precipitation couples the magnetosphere, ionosphere, and atmosphere together, affecting ionospheric conductance, outflow, chemistry, and many other areas of interest. Even lacking morphological detail (as all current

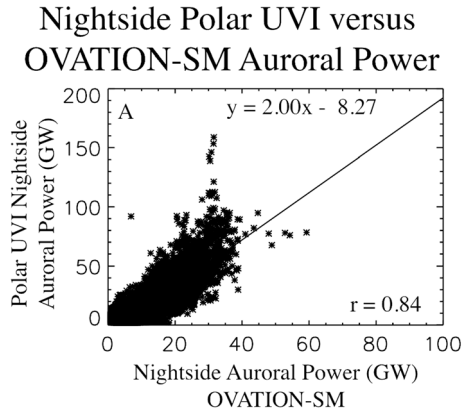


**Figure 6.** Polar UVI nightside auroral power versus OVATION-SM nightside auroral power.

models do), an auroral model can be extremely useful if it captures hemispheric auroral power. *Newell et al.* [2010a] examined four major auroral models, comparing the hemispheric nightside auroral power predicted by the models with the hemispheric nightside auroral power captured by Polar UVI. They found that OVATION Prime accounted for 56% of the variance in Polar UVI on a minute-by-minute basis for both recurrent and isolated substorms and intervals between substorms.

[54] To validate OVATION-SM, the Polar UVI hemispheric nightside auroral power is compared with the hemispheric nightside auroral power from OVATION-SM as well as the four models considered by *Newell et al.* [2010a] as reference values. All five models and Polar UVI have to contain valid data for the data point to be used. For example, if the solar wind conditions are not available for a specific time or if it is not an isolated substorm, then the data are not used from any of the models or Polar UVI. Under these conditions, 25,255 points of comparison from December 1996 thru December 1997 are identified. The results for Polar UVI hemispheric nightside auroral power versus OVATION-SM hemispheric nightside auroral power are shown in Figure 6. The linear fit and correlation coefficient for Polar UVI hemispheric nightside auroral power versus each model is calculated. The linear fit has a slope of  $\sim 2$ ; this slope may occur from the lack of calibration between Polar UVI data and DMSP data [*Newell et al.*, 2010a]. The square of the correlation coefficient (or the variance) is also calculated for each comparison. OVATION-SM nightside auroral power accounts for 71% of the variance in the Polar UVI nightside auroral power, a large increase over OVATION Prime and the other auroral models. Table 1 gives the percentage of variance in Polar UVI hemispheric nightside auroral power accounted for by each model under the same conditions. The Hardy  $Kp$  model is the lowest accounting for only 37%, while OVATION Prime is the closest to OVATION-SM at 47%.

#### 4. Features of OVATION-SM

[55] There are some interesting features in OVATION-SM, including the well-organized bands where stepwise regression selects a time variable first in ion and diffuse

electron auroras. These areas suggest more study is needed to elucidate understanding.

[56] DMSP data from 1984 to 2005 are used along with OVATION-SM to elucidate the role of substorm phase (as represented by time) in these features. The DMSP data are split into auroral type, geomagnetic bin (MLT and MLAT), and 2 min bins from 90 min prior to onset to 90 min post-onset. The DMSP data are the same data used in creating the OVATION-SM model; i.e., the data are from isolated substorms occurring between 1984 and 2005. Time to onset was the only criteria for separating, thus the SME index value may be any value for these data.

[57] OVATION-SM is run for the 14,434 substorms. The results are split into auroral type, geomagnetic bin (MLT and MLAT), and 2 min bins from 90 min prior to onset to 90 min post-onset. The superposed epoch of the SME indices for the 14,434 substorms is shown in Figure 7. The SME indices increase slightly prior to onset, then jump 200 nT at onset before peaking  $\sim 20$  min after onset.

[58] Discussion of several points has been deferred for this section, including the following:

[59] 1. time dependencies in nightside auroral activity (ion and diffuse electron);

[60] 2. dayside diffuse electron aurora, specifically the band where the time since last substorm onset ( $T_1$ ) is chosen first by stepwise regression from 0500 to 1600 MLT. The expectation is that auroral power decreases with increasing time since last substorm onset ( $T_1$ ) within this band; and

[61] 3. the band where time until next substorm ( $T_2$ ) is chosen first by stepwise regression in ion aurora, wrapping from 0500 to 2300 MLT. This band corresponds to the well-defined edge between high and low correlation. It has been suggested that the well-defined edge is the result of a nonlinear response between DMSP ion energy flux and onset timing.

[62] Taking each auroral type individually, the superposed epochs of the model results are compared with DMSP data. Figures 8–11 illustrate these results. The results will be discussed qualitatively. The purpose of this section is to show OVATION-SM has some interesting features. By the end of section 4, the reader should see that the OVATION-SM model provides a few new and insightful details.

#### 4.1. Nightside Auroral Activity

[63] DMSP nightside diffuse electron auroral power shows a substorm signature (Figure 8a), rising at onset and peaking  $\sim 30$  min after onset. OVATION-SM predicts a comparable nightside diffuse electron auroral power, peaking at  $\sim 16$  GW (Figure 8b, black trace). The total auroral power for the model components is provided (the constant in red; the SME indices

**Table 1.** Percentage of Variance of Polar UVI Nightside Auroral Power Accounted for by Specified Model

Models	Percentage of Variance Accounted for by Model
Hardy $Kp$ Model	37%
Brautigam IMF-Based Model	39%
Evans Nowcast Model	43%
OVATION Prime	47%
OVATION-SM	71%

### Superposed Epoch of SuperMAG SME Index

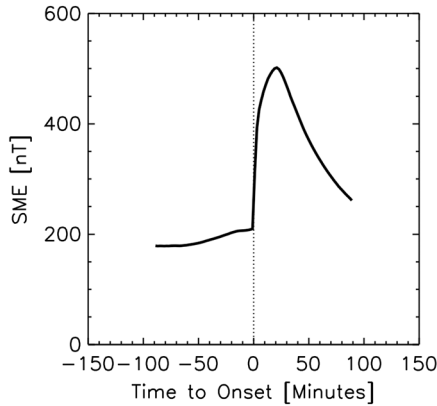


**Figure 7.** Superposed epoch of SME indices for 14,434 substorms between 1984 and 2005. Substorm onset is marked by a dashed vertical line.

in blue; the combination of times in green). The time variables cause a decrease in the total auroral power prior to onset when time since last substorm onset is dominant. Post-onset, the time variables provide an increase in the total power. The effects of the time variables are very small, overall.

[64] DMSP nightside ion auroral power responds to onset (Figure 8c), rising ~0.5 GW as seen by *Newell et al.* [2010c]. OVATION-SM predicts similar nightside ion auroral power (Figure 8d, black trace) with a peak value of ~3.1 GW. The change in the total auroral power from the time variables is minimal, decreasing the total auroral power except for the first 35 min post-onset.

[65] OVATION-SM results increase prior to onset. While the increase is ~0.1 GW, this increase prompts examination of nightside DMSP data for a similar trend. If there is indeed an increase in ion auroral precipitation prior to onset as OVATION-SM suggests, data should indicate a growth in auroral power if binned by time. The DMSP nightside ion auroral power shows a possible trend (Figure 8c), but it is not clear.

[66] Figure 9 shows five DMSP ion auroral energy flux maps, each containing the data for a 2 min bin. The line graph

### Nightside Ion & Diffuse Electron Auroral Power

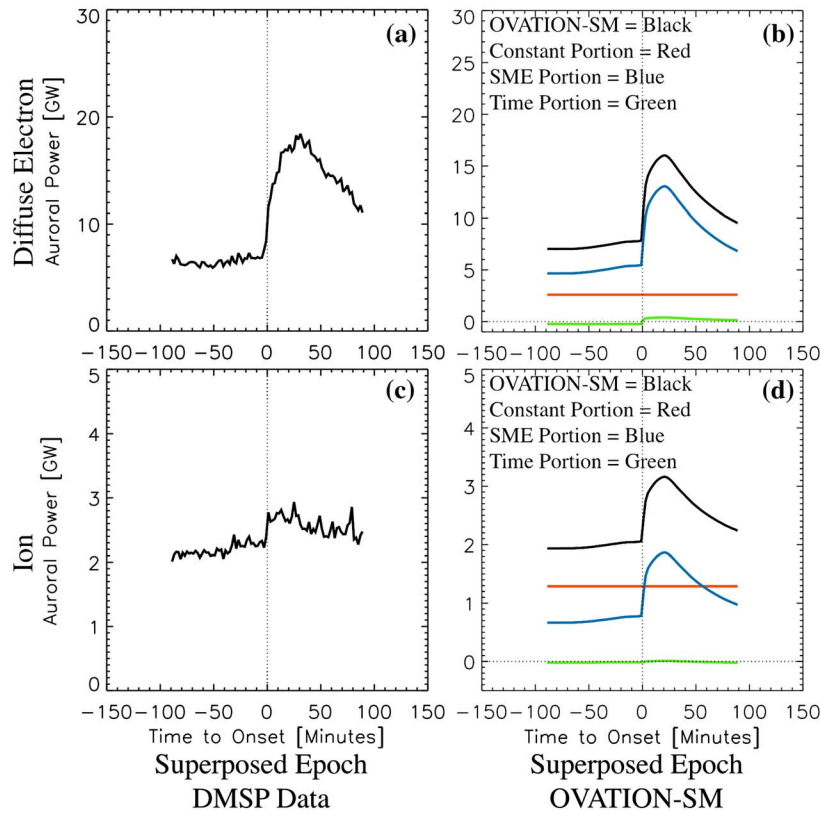


**Figure 8.** Nightside (1800–0600 MLT, 60°–80° MLAT) (a and b) diffuse electron and (c and d) ion auroral power. Diffuse electron auroral power superposed epoch DMSP data centered on substorm onset (Figure 8a). Diffuse electron auroral power superposed epoch OVATION-SM results centered on substorm onset (Figure 8b). Ion auroral power from superposed epoch DMSP data centered on substorm onset (Figure 8c). Ion auroral power from superposed epoch OVATION-SM results centered on substorm onset (Figure 8d). Black line represents OVATION-SM results, red lines represent the contribution of the constant to the total auroral power, blue lines represent the contribution of the SME indices to the total auroral power, and the green lines represent the contribution of the time variables to the total auroral power.

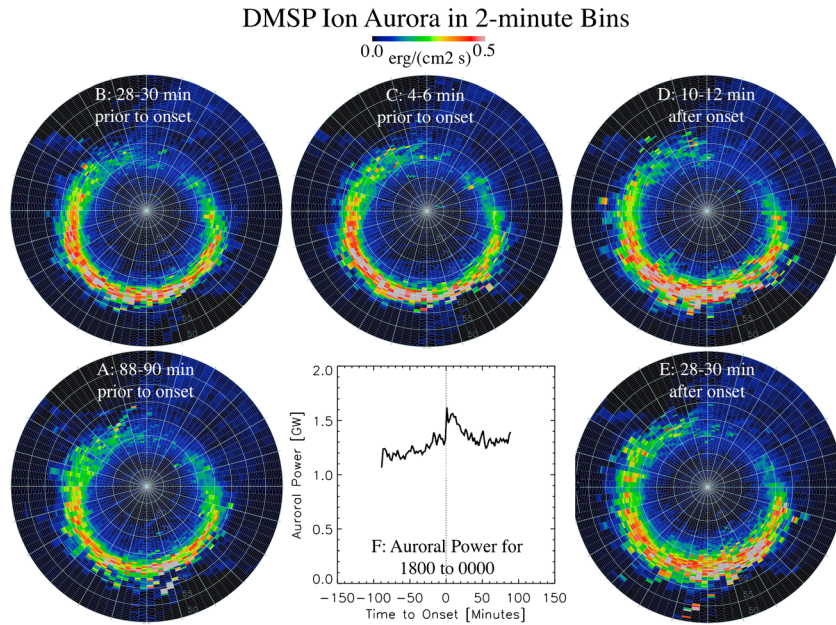


**Figure 9.** DMSP ion auroral energy flux maps binned in 2 min aggregates for (a) 88–90 min prior to substorm onset, (b) 28–30 min prior to substorm onset, (c) 4–6 min prior to substorm onset, (d) 10–12 min after substorm onset, and (e) 28–30 min after substorm onset. (f) Premidnight DMSP ion auroral power for 2 min bins between 90 min prior to substorm onset and 90 min after substorm onset.

in Figure 9 is the DMSP premidnight ion auroral power. There is a noticeable increase in the DMSP premidnight ion auroral power prior to onset (Figure 9f). The premidnight DMSP ion auroral power trends much closer to the superposed epoch of SME indices than the nightside ion auroral power does.

[67] The DMSP ion auroral energy flux maps for times prior to onset show the increase in energy flux in the premidnight sector also (Figures 9a–9e). The increase covers most of the premidnight sector.

[68] The exact timing of this increase in ion auroral precipitation is beyond the scope of this current version of

OVATION-SM and the current handling of the DMSP data. OVATION-SM does not have the ability to resolve fine structure either spatially, as shown in section 3.2, or temporally, due to substorm onset timing and statistical nature of data. The DMSP data used are an averaged conglomeration of all ion auroral precipitation that occurred in the particular time bin in question. Thus, while being able to say, there is an increase in ion aurora energy flux to explore, it is impossible to say more.

[69] An increase in ion auroral precipitation should not be a surprise to the field. Several studies have seen an increase in ion auroras 30–60 min prior to substorm onset [e.g.,

### Dayside Diffuse Electron Auroral Power

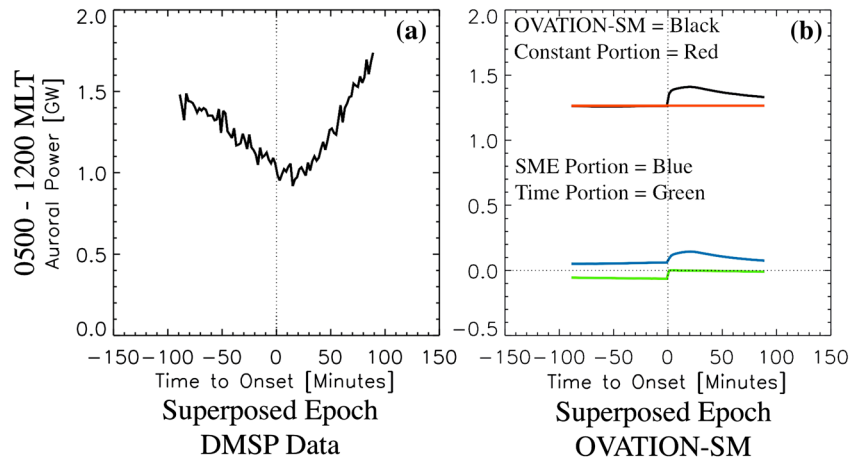


**Figure 10.** Morning (0500–1200 MLT, 70°–75° MLAT) diffuse electron auroral power. (a) Superposed epoch DMSP data centered on substorm onset. (b) Superposed epoch OVATION-SM results centered on substorm. Black line represents OVATION-SM results, red lines represent the contribution of the constant to the total auroral power, blue lines represent the contribution of the SME indices to the total auroral power, and the green lines represent the contribution of the time variables to the total auroral power.

## Ion Auroral Power for Band of Time Variables

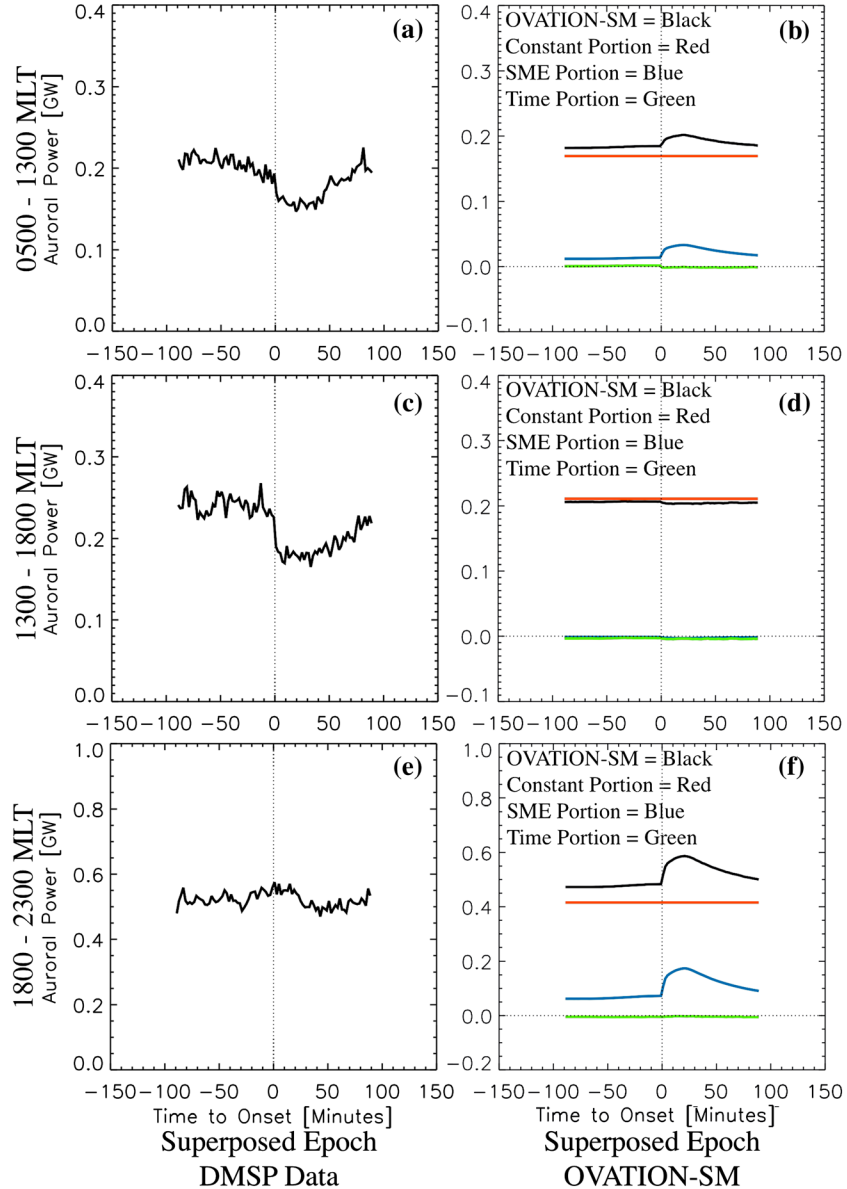


**Figure 11.** Ion auroral power for time-dependent swath. (a and b) Morning (0500–1300 MLT,  $72^{\circ}$ – $77^{\circ}$  MLAT), (c and d) afternoon (1300–1800 MLT,  $70^{\circ}$ – $75^{\circ}$  MLAT), and (e and f) evening (1800–2300 MLT,  $65^{\circ}$ – $70^{\circ}$  MLAT) ion auroral power. Superposed epoch DMSP data centered on substorm onset (Figures 11a, 11c, and 11e). Superposed epoch OVATION-SM results centered on substorm onset (Figures 11b, 11d, and 11f). Black line represents OVATION-SM results, red lines represent the contribution of the constant to the total auroral power, blue lines represent the contribution of the SME indices to the total auroral power, and the green lines represent the contribution of the time variables to the total auroral power.

*Mende et al.*, 2002, 2003; *Jahn et al.*, 2006]. *Jahn et al.* [2006] discussed the increased ion auroras in terms of the neutral atom emissions, suggesting that the behavior mimics pseudobreakups seen in ion auroras. *Mende et al.* [2003] showed ion auroral precipitation occurring prior to onset using IMAGE. They also showed the ion auroral boundary moving equatorward pre-onset and then rebounding along with the electron precipitation poleward. The DMSP ion auroral energy flux maps in Figure 9 also show ion auroral precipitation suddenly expanding poleward after onset. This

observation brings the discussion full circle to the correlations seen in Figure 2d, where ion auroral energy flux has a lower correlation on the poleward side of the auroral oval. This is one more piece of evidence toward a nonlinear response at onset, which is captured by a time-dependent auroral precipitation model.

#### 4.2. Dayside Diffuse Electron Aurora

[70] Dayside diffuse electron auroras contain a swath where time since last substorm onset ( $T_1$ ) is chosen first by

stepwise regression (Figure 4, 0500–1200 MLT, 70°–75° MLAT and 1200–1600 MLT, 65°–75° MLAT). The portion of the swath between 0500 and 1200 MLT coincides with the area where all three variables are statistically significant. DMSP diffuse auroral power from this swath shows a very different signature than seen so far (Figure 10a). The swath has decreasing auroral power prior to onset, which correlates to increasing time since last substorm onset ( $T1$ ). This result was predicted in 3.1. As electrons enter the inner magnetosphere and drift eastward, they encounter changing magnetic fields, which cause some to drift into the loss cone and precipitate. The drop-off in auroral power fits this theory. The electron population would decrease both as it drifts eastward (drop in afternoon power compared to prenoon [not shown]) and as time from substorm onset increases. The onset of a new substorm would replenish the supply of electrons but not immediately, hence the 15–20 min offset in the dayside minimum.

[71] OVATION-SM results do not agree with the DMSP data (Figure 10b, black trace). OVATION-SM captures the correct auroral power range, but it misses the trend. OVATION-SM results are flat pre-onset while data decrease, and the results increase at onset instead of 15–20 min after onset. When the effects on the total auroral power are separated by variables, the portion due to time variables (green trace) causes a decrease in the total prior to onset ( $T1$  dominant). This decrease is offset by the portion of the total auroral power due to the SME indices (blue trace). Just post-onset, the portion of total auroral power due to time variables (green trace) has no effect on the total auroral power ( $T2$  dominant). The SME index influence is still strong. Dayside diffuse electron auroras in OVATION-SM might do much better with the inclusion of an MLT-dependent magnetic perturbation (local SME).

#### 4.3. Dayside Ion Aurora

[72] Unlike the other auroral types, ion auroras appear to have an organized band in both the dayside and nightside where time until next substorm onset ( $T2$ ) is the first chosen variable (Figure 4d). The band goes from 0500 to 2300 MLT and from 77° to 65° MLAT. Separating it into three sections (0500–1300 MLT, 72°–77° MLAT; 1300–1800 MLT, 70°–75° MLAT; and, 1800–2300 MLT, 65°–70° MLAT), the DMSP auroral power for each section is plotted in Figures 11a, 11c, and 11e, respectively. The DMSP auroral power does not spike just post-onset, but rather remains stable (nightside) or decreases (dayside). These decreases are large for ion auroras (about 0.05 to 0.10 GW), but they are small compared to diffuse electron auroral power.

[73] OVATION-SM results for the prenoon and premidnight sections increase post-onset (Figures 11b and 11f, black traces). The postnoon section in OVATION-SM decreases post-onset, capturing the DMSP data response (Figure 11d, black traces). The prenoon auroral power dependent on the time variables in OVATION-SM increases the total auroral power prior to onset and decreases the total auroral power after onset (Figure 11b, green trace). Both the postnoon auroral power dependent on the time variables and on the SME indices decrease the total auroral power; the magnitude of the decrease grows post-onset (Figure 11d, green and blue traces). The nightside auroral power dependent on the time variables decreases the total auroral power constantly. The portions of

the auroral power dependent on time variables trend similar to the DSMP data binned by time to and from onset. This suggests that the time variables provide an important feature in OVATION-SM and that the use of a local SME index might help achieve a better dayside auroral power estimate.

[74] One of the most interesting features of this organized band (where time until the next substorm onset ( $T2$ ) is the first chosen variable out of the three) is its collocation with the well-defined drop in correlation (Figure 2d). When this band is highlighted in the auroral energy flux maps from the DMSP data (Figures 9a–9e), the band collocates with the ion aurora boundary prior to onset. It is only post-onset that any increase in the measure of ion auroral energy flux is seen poleward of this band. This ion auroral boundary is a new feature of OVATION-SM.

## 5. Conclusions

[75] OVATION-SM, an empirical model for different types of auroral energy flux, has been developed. OVATION-SM is a linear combination of the SME index (or square root of SME index for monoenergetic auroras), time since the last substorm onset, and time until the next substorm onset. Because OVATION-SM is based on ground magnetometer data and products of that data, it is possible to calculate continuous auroral power at a 1 min cadence for 30+ years.

[76] OVATION-SM captures the gross auroral morphology, including onsets and other brightening and dimming events. The detailed auroral morphology (i.e., streamers and arcs) is beyond the scope of the current version of OVATION-SM. This is not surprising as OVATION-SM is based on location-independent variables, and detailed morphology will require MLT-dependent variables.

[77] OVATION-SM explains more than 70% of the variance in Polar UVI nightside auroral power, which makes it a better predictor of nightside auroral power than any other model currently available.

[78] The OVATION-SM model provides minute-by-minute representations of ionospheric auroral energy flux for each auroral type (monoenergetic, broadband, diffuse electron, and ion). OVATION-SM models nightside auroral precipitation well, capturing substorm trends for all auroral types.

[79] OVATION-SM does not model dayside auroral precipitation as well. OVATION-SM captures the loss process for diffuse electron precipitating through the loss cone as they drift eastward. While the trend in auroral power is not accurately predicted, the magnitude of loss is the same order as seen in data.

[80] OVATION-SM captures both precipitation of ion aurora and the poleward ion auroral boundary prior to onset.

[81] Overall, OVATION-SM is a great addition to the tools with which substorms and auroral precipitation are studied. It provides a more accurate portrayal of the auroral energy flux than any previous model and can be run for any time period for which the SuperMAG database is available.

## 6. Future Work

[82] In its current form, OVATION-SM gives good nightside auroral power measurements but does not capture any of the morphology of the auroras. The lack of morphology is a direct result of using location-independent variables to

predict local changes. To make a more morphologically accurate model, local magnetometer readings are needed. The next step in the evolution of OVATION-SM is to add the local magnetometer readings, thus adding location-dependent details to the individual auroral types as well as to the total auroras predicted.

[83] In addition to evolving OVATION-SM, the current version of OVATION-SM will be added to the SuperMAG website in the form of nightside auroral power line plots for 1980 to 2009.

[84] **Acknowledgments.** This work was supported in part by NSF grants ANT-1043010, AGS-1132361, and AGS-1045638 to the Johns Hopkins University. For the ground magnetometer data, we gratefully acknowledge the following: Intermagnet; USGS, Jeffrey J. Love; Danish Meteorological Institute; CARISMA, PI Ian Mann; CANMOS; The S-RAMP Database, PI K. Yumoto, and Dr. K. Shiokawa; The SPIDR database; AARI, PI Oleg Troshichev; The MACCS program, PI M. Engebretson, Geomagnetism Unit of the Geological Survey of Canada; GIMA; MEASURE, UCLA IGPP, and Florida Institute of Technology; SAMBA, PI Eftyhia Zesta; 210 Chain, PI K. Yumoto; SAMNET, PI Farideh Honary; the institutes who maintain the IMAGE magnetometer array, PI Eija Tanskanen; PENGUIN; AUTUMN, PI Martin Connors; Greenland magnetometers operated by DTU Space; South Pole and McMurdo Magnetometer, PI's Louis J. Lanzarotti, and Alan T. Weatherwax; ICESTAR; RAPIDMAG; PENGUIn; British Antarctic Survey; McMac, PI Peter Chi; BGS, PI Susan Macmillan; Pushkov Institute of Terrestrial Magnetism, Ionosphere and Radio Wave Propagation (IZMIRAN); SuperMAG, PI Jesper W. Gjerloev.

[85] Robert Lysak thanks the reviewers for their assistance in evaluating this paper.

## References

- Brautigam, D. H., M. S. Gussenhoven, and D. A. Hardy (1991), A statistical study on the effects of IMF Bz and solar wind speed on auroral precipitation, *J. Geophys. Res.*, *96*, 5525, doi:10.1029/91JA00157.
- Chaston, C. C., J. W. Bonnell, C. W. Carlson, J. P. McFadden, R. E. Ergun, and R. J. Strangeway (2003), Properties of small-scale Alfvén waves and accelerated electrons from FAST, *J. Geophys. Res.*, *108*(A4), 8003, doi:10.1029/2002JA009420.
- Chaston, C. C., J. W. Bonnell, C. W. Carlson, J. P. McFadden, R. E. Ergun, R. J. Strangeway, and E. J. Lund (2004), Auroral ion acceleration in dispersive Alfvén waves, *J. Geophys. Res.*, *109*, A04205, doi:10.1029/2003JA010053.
- Chaston, C. C., C. W. Carlson, J. P. McFadden, R. E. Ergun, and R. J. Strangeway (2007), How important are dispersive Alfvén waves for auroral particle acceleration?, *Geophys. Res. Lett.*, *34*, L07101, doi:10.1029/2006GL029144.
- Christon, S. P., D. J. Williams, D. G. Mitchell, C. Y. Huang, and L. A. Frank (1991), Spectral characteristics of plasma sheet ion and electron populations during disturbed geomagnetic conditions, *J. Geophys. Res.*, *96*, 1, doi:10.1029/90JA01633.
- Davis, T. N., and M. Sugiura (1966), Auroral electrojet activity index AE and its universal time variations, *J. Geophys. Res.*, *71*, 785.
- Evans, D. S. (1987), Global statistical patterns of auroral phenomena, in *Quantitative Modeling of Magnetospheric-Ionospheric Coupling Processes*, edited by Y. Kamide and R. A. Wolfe, p. 325, Kyoto Sangyo Univ., Kyoto, Japan.
- Fillingim, M. O., G. K. Parks, H. U. Frey, T. J. Immel, and S. B. Mende (2005), Hemispheric asymmetry of the afternoon electron aurora, *Geophys. Res. Lett.*, *32*, L03113, doi:10.1029/2004GL021635.
- Frank, L. A., and K. L. Ackerson (1971), Observations of charged particle precipitation into the auroral zone, *J. Geophys. Res.*, *76*(16), 3612, doi:10.1029/JA076i016p03612.
- Gjerloev, J. W. (2012), The SuperMAG data processing technique, *J. Geophys. Res.*, *117*, A09213, doi:10.1029/2012JA017683.
- Hardy, D. A., M. S. Gussenhoven, and E. Holeman (1985), A statistical model of auroral electron precipitation, *J. Geophys. Res.*, *90*, 4229, doi:10.1029/JA090iA05p04229.
- Hardy, D. A., W. McNeil, M. S. Gussenhoven, and D. Brautigam (1991), A statistical model of auroral ion precipitation: 2. Functional representation of the average patterns, *J. Geophys. Res.*, *96*, 5539.
- Holland, R. F. (1969), Excitation of nitrogen by electrons: The Lyman-Birge-Hopfield system of N<sub>2</sub>, *J. Chem. Phys.*, *51*, 3940.
- Jahn, J.-M., C. J. Pollock, T. J. Immel, and S. B. Mende (2006), Spatial correlation of precipitating and trapped protons associated with an isolated substorm, *Geophys. Res. Lett.*, *33*, L15102, doi:10.1029/2006GL025917.
- Kletzing, C. A., J. D. Scudder, E. E. Dors, and C. Curto (2003), The auroral source region: Plasma properties of the high altitude plasma sheet, *J. Geophys. Res.*, *108*(A10), 1360, doi:10.1029/2002JA009678.
- Liou, K. and P. T. Newell (2010), On the azimuthal location of auroral breakup: Hemispheric asymmetry, *Geophys. Res. Lett.*, *37*, L23103, doi:10.1029/2010GL045537.
- Liou, K., P. T. Newell, C.-I. Meng, M. Brittnacher, and G. Parks (1997), Synoptic auroral distribution: A survey using Polar ultraviolet imagery, *J. Geophys. Res.*, *102*(A12), 27,197.
- Liou, K., P. T. Newell, C.-I. Meng, M. Brittnacher, and G. Parks (1998), Characteristics of the solar wind controlled auroral emissions, *J. Geophys. Res.*, *103*, 17,543, doi:10.1029/98JA01388.
- Mende, S. B., H. U. Frey, T. J. Immel, D. G. Mitchell, P. C. son-Brandt, and J.-C. Gerard (2002), Global comparison of magnetospheric ion fluxes and auroral precipitation during a substorm, *Geophys. Res. Lett.*, *29*(12), 1609, doi:10.1029/2001GL014143.
- Mende, S. B., H. U. Frey, B. J. Morosony, and T. J. Immel (2003), Statistical behavior of proton and electron auroras during substorms, *J. Geophys. Res.*, *108*(A9), 1339, doi:10.1029/2002JA009751.
- Newell, P. T., and J. W. Gjerloev (2011a), Evaluation of SuperMAG auroral electrojet indices as indicators of substorms and auroral power, *J. Geophys. Res.*, *116*, A12211, doi:10.1029/2011JA016779.
- Newell, P. T., and J. W. Gjerloev (2011b), Substorm and magnetosphere characteristic scales inferred from the SuperMAG auroral electrojet indices, *J. Geophys. Res.*, *116*, A12232, doi:10.1029/2011JA016936.
- Newell, P. T., K. Liou, T. Sotirelis, and C.-I. Meng (2001), Auroral precipitation power during substorms: A Polar UV Imager-based superposed epoch analysis, *J. Geophys. Res.*, *106*(A12), 28,885, doi:10.1029/2000JA000428.
- Newell, P. T., T. Sotirelis, and S. Wing (2009), Diffuse, monoenergetic, and broadband aurora: The global precipitation budget, *J. Geophys. Res.*, *114*, A09207, doi:10.1029/2009JA014326.
- Newell, P. T., T. Sotirelis, K. Liou, A. R. Lee, S. Wing, J. Green, and R. Redmon (2010a), Predictive ability of four auroral precipitation models as evaluated using Polar UVI global images, *Space Weather*, *8*, S12004, doi:10.1029/2010SW000604.
- Newell, P. T., T. Sotirelis, and S. Wing (2010b), Seasonal variations in diffuse, monoenergetic, and broadband aurora, *J. Geophys. Res.*, *114*, A03216, doi:10.1029/2009JA014805.
- Newell, P. T., A. R. Lee, K. Liou, S.-I. Ohtani, T. Sotirelis, and S. Wing (2010c), Substorm cycle dependence of various types of aurora, *J. Geophys. Res.*, *115*, A09226, doi:10.1029/2010JA015331.
- Strickland, D. J., J. R. Jasperse, and J. A. Whalen (1983), Dependence of auroral FUV emissions on the incident electron spectrum and neutral atmosphere, *J. Geophys. Res.*, *88*(A10), 8051.
- Torr, M. R., et al. (1995), A far ultraviolet imager for the international solar-terrestrial physics mission, *Space Sci. Rev.*, *71*, 329.
- Wing, S., and P. T. Newell (1998), Central plasma sheet ion properties as inferred from ionospheric observations, *J. Geophys. Res.*, *103*, 6785, doi:10.1029/97JA02994.